The role of halogens in on-surface Ullmann polymerization

Gianluca Galeotti, Marco Di Giovannantonio, Josh Lipton-Duffin, Maryam Ebrahimi, Stefano Tebi, Alberto Verdini, Luca Floreano, Yannick Fagot-Revurat, Dmitrii F. Perepichka, Federico Rosei, et al.

Faraday Discussions

Cite this: *Faraday Discuss.*, 2017, **204**, 453

The role of halogens in on-surface Ullmann polymerization†

Gianluca Galeotti,[a] Marco Di Giovannantonio,[‡b] Josh Lipton-Duffin,[c] Maryam Ebrahimi,[*a] Stefano Tebi,[b] Alberto Verdini,[d] Luca Floreano,[d] Yannick Fagot-Revurat,[e] Dmitrii F. Perepichka,[f] Federico Rosei[*a] and Giorgio Contini[*bg]

Received 9th March 2017, Accepted 30th March 2017

DOI: 10.1039/c7fd00099e

Ullmann coupling is the most common approach to form surface-confined one- and two-dimensional conjugated structures from haloaryl derivatives. The dimensions of the formed nanostructures can be controlled by the number and location of halogens within the molecular precursors. Our study illustrates that the type of halogen plays an essential role in the design, orientation, and extent of the surface-confined organometallic and polymeric nanostructures. We performed a comparative analysis of five 1,4-dihalobenzene molecules containing chlorine, bromine, and iodine on Cu(110) using scanning tunneling microscopy, fast-X-ray photoelectron and near edge X-ray absorption fine structure spectroscopies. Our experimental data identify different molecular structures, reaction temperatures and kinetics depending on the halogen type. Climbing image nudged elastic band simulations further clarify these observations by providing distinct diffusion paths for each halogen species. We show that in addition to the structure of the building blocks, the halogen type has a direct influence on the morphology of surface-confined polymeric structures based on Ullmann coupling.

[a]*Centre Énergie, Matériaux et Télécommunications, Institut National de la Recherche Scientifique, 1650 Boulevard Lionel-Boulet, Varennes, QC, J3X 1S2, Canada. E-mail: rosei@emt.inrs.ca; maryam.ebrahimi@emt.inrs.ca*

[b]*Istituto di Struttura della Materia, CNR, Via Fosso del Cavaliere 100, 00133 Roma, Italy. E-mail: giorgio.contini@cnr.it*

[c]*School of Chemistry, Physics and Mechanical Engineering, Institute for Future Environments, Queensland University of Technology (QUT), 2 George Street, Brisbane, QLD 4001, Australia*

[d]*Istituto Officina dei Materiali CNR, Laboratorio TASC, s.s. 14 km 163.5, 34149 Trieste, Italy*

[e]*Institut Jean Lamour, UMR 7198, Université Lorraine/CNRS, B.P. 239 FE-54506, Vandoeuvre-les-Nancy, France*

[f]*Department of Chemistry, McGill University, 801 Sherbrooke Str. West, Montreal, QC H3A 0B8, Canada*

[g]*Department of Physics, University of Rome Tor Vergata, Via della Ricerca Scientifica 1, 00133 Roma, Italy*

† Electronic supplementary information (ESI) available. See DOI: 10.1039/c7fd00099e

‡ Present address: Empa – Swiss Federal Laboratories for Materials Science and Technology, Überlandstrasse 129, 8600 Dübendorf, Switzerland.

Introduction

The discovery of graphene, an atomically thin layer of carbon which exhibits remarkable thermal, mechanical, and optoelectronic properties, highlights the greatest breakthrough in materials science of the past decade.[1–4] However, graphene's zero bandgap limits its application as a semiconductor in electronic devices, which has stimulated a growing interest to synthesize organic analogues of graphene.[5–9] One of the most compelling strategies in this arena is to design surface-confined fully-conjugated polymers with tunable bandgaps based on a rational choice of monomer.[10–13] The flexibility of organic synthesis offers a broad playground for creating two-dimensional (2D) conjugated polymers by exploring various surface reactions using different building blocks.[14–17] Surface-confined 2D polymers may be synthesized through bottom-up methodologies which yield large molecular structures resulting from small monomers.[10] The surface acts as template, creating ordered 1D[18] or 2D[19] polymeric structures by suppressing the entropically-driven disorder of solution synthesis.

In addition to passive templating, the surface can also act as a catalyst, accelerating the reaction and guiding the orientation of the growing polymer structure.[20] Although it is relatively easy to obtain long-range order in self-assembled molecular networks (SAMNs) which are driven by weak intermolecular interactions, this is rarely the case for covalently bound structures, due to the irreversible nature of covalent coupling. A possible approach to forming long-range ordered covalent networks is to use a multi-step reaction, in which the monomers first form a dynamic intermediate which arranges into a 2D monolayer. The neighboring molecules can subsequently undergo a coupling reaction forming a polymer made of covalent C–C bonds.[21,22] Ullmann coupling, the most popular reaction used in on-surface chemistry, expresses these features, it is a two-step process in which the transition metal supporting substrate catalyzes[23] the dehalogenation of aryl halide precursors, forming an organometallic (OM) intermediate[18] which subsequently couples into a covalent structure *via* new C–C bonds.[24] The activation energy of the reaction depends on both the particular molecule[25] and the surface.[26,27] On Cu and Ag surfaces, the deposited molecules can dehalogenate at room temperature (RT) and form an OM intermediate phase that is stable up to the polymerization temperature.[28–30]

While the majority of recent studies on surface-confined Ullmann coupling focused on understanding the structure and order of the polymers on different substrates[27] and the density of defects,[31] the effects of the halogen by-product have not been explored in detail. A few theoretical[20] and experimental[32,33] studies have reported the dissociation of halobenzenes on metallic surfaces, addressing the differences in the adsorption energies. However, the effects of halogens on the reaction outcome have not been explored. The derivatives of 1,3,5-tris(4-halophenyl)benzene functionalized with bromine (TBB),[26,34] iodine (TIB),[25] and both halogens (TBIB)[30] have been studied on various surfaces, yet a coherent comparison to reveal the role played by the halogens was not reported. Our recent work described the contribution of halogens in the formation of 1D polymers *via* Ullmann coupling,[28,29] showing that the halogens are part of the OM unit cell after the deposition of 1,4-dibromobenzene (dBB) on Cu(110). These studies also illustrate that the structures obtained from dBB[28] and 1,4-

diiodobenzene (dIB)[18] on Cu(110) are different, which suggests the importance of studying the influence of halogens on the processes that transform the intermediate phase into a polymeric structure.

Since the first report describing on-surface Ullmann coupling under ultra-high vacuum (UHV) conditions,[35] several studies have provided insights into its reaction mechanisms and kinetics.[23,24,36] A kinetic model based on a combined experimental and theoretical approach was applied to the polymerization of dBB on Cu(110), showing that the reaction follows a nucleation-and-growth mechanism.[37] However, there are still open questions regarding both the fundamental understanding and the practical realization of on-surface Ullmann coupling.[38] In line with this perspective, we address how the type of halogen can influence the design of the OM and polymer structures.

Here, we report a systematic study of five different 1,4-dihalobenzene molecules, a phenyl ring containing two halogens (Cl, Br or I) located at the *para* positions, on Cu(110). Our findings illustrate the role of the metal halide byproduct in determining the rate of C–C coupling step and the order of the formed π-conjugated polymers based on Ullmann coupling.

Materials and methods

All experiments were performed under UHV conditions with base pressures below 2×10^{-10} mbar. The precursors dBB (98% purity), dIB (99%), 1,4-dichlorobenzene (dCB, ≥99%), 1-bromo-4-chlorobenzene (BCB, 99%) and 1-bromo-4-iodobenzene (BIB, 98%), shown in Fig. 4, were purchased from Sigma-Aldrich and were deposited through a leak valve onto Cu(110) (MaTecK GmbH), with the substrate held at RT. All experiments were performed starting from a saturated monolayer coverage. The substrate was prepared by repeated cycles of Ar^+ sputtering (1.2 keV) and annealing (500 °C). Scanning tunneling microscopy (STM) was performed at RT in constant-current mode using an Omicron VT-STM. Quoted bias voltages are measured from the tip to the sample. STM images were analyzed using WSxM,[39] and were treated for plane subtraction, line-by-line flattening, contrast enhancement, and were corrected based on the known lattice parameters of the substrate. X-ray photoelectron spectroscopy (XPS), fast-XPS and near edge X-ray absorption fine structure (NEXAFS) spectroscopy measurements were performed at the ALOISA beamline of the Elettra synchrotron-radiation facility in Trieste (Italy). XPS experiments were performed in normal emission geometry, with a 4° grazing incidence of linearly polarized radiation, using a pass energy of 18 eV and a home-built hemispherical electron analyzer equipped with a multichannel plate (MCP) detector. The C 1s, Br 3d and Cl 2p core levels were measured at a photon energy of 390 eV with an overall energy resolution of 200 meV. The I 3d peak was measured at a photon energy of 750 eV with an overall energy resolution of 300 meV. Unless stated otherwise, the spectral peak fitting based on residual minimization with Gaussian–Lorentzian line shape functions (30% Lorentzian) and linear backgrounds was performed using Casa XPS[40] and CONTUR[41] software.

The fast-XPS maps of C 1s were acquired by increasing the sample temperature from RT to 230 °C with a heating rate of 0.2 °C s^{-1}, using a radiative heating element behind the sample. Every line on each map is a snapshot of the C 1s peak, taken at the rate of one spectrum per second at a photon energy of 390 eV and

pass energy set to 30 eV (overall energy resolution of ~350 meV). The NEXAFS C K-edge spectra were recorded in partial electron yield by means of a channeltron equipped with a filtering grid biased at 240 V, to reject the tail of secondary electrons. The photon energy resolution was set to 100 meV. To calibrate the photon energy scale, the drain current on the last refocusing mirror of the beamline was measured along with the C K-edge, and subsequently calibrated back to reference data. The C K-edge spectrum acquired from the clean Cu(110) surface was used to normalize the spectra from surfaces containing the molecular layers. Polarization dependent measurements were performed by rotating the sample about the beam axis, changing the angle (θ) of the surface with respect to the polarization vector from transverse magnetic (TM, almost p-polarization) to transverse electric (TE, s-polarization) geometry, while keeping the grazing photon incidence angle fixed at 6° (see Floreano *et al.*[42] for details about NEXAFS geometry and calibration).

Density functional theory (DFT) calculations were performed with the Vienna Ab-initio Simulation Package (VASP)[43,44] installed at the SciNet[45] supercomputer clusters of Compute Canada. DFT calculations were executed using the Perdew–Burke–Ernzerhof approximation (PBE)[46] of the exchange–correlation potential, the projector augmented wave (PAW)[47,48] method, and a plane-wave basis set with an energy cut off of 450 eV. Final calculations were performed using the zero-damping DFT-D3 [49] methods of Grimme, in which vdW correction for potential energy and dispersion effects are taken into account *via* a semi-empirical approach. The *k*-point sampling was restricted to the Γ point to cope with the large size of the supercells. The energy barriers for the diffusion of the halogens (Cl, Br, I) were determined by calculating the minimum energy pathways (MEPs) along the [001], [1−10], [1−12], and [1−11] surface directions using the climbing image nudged elastic band (CI-NEB) method.[50,51] For the initial states, the most stable geometry/location of the halogen was found to be short-bridge for Cl and Br, and hollow for I. The path of diffusion from the initial state to the nearest similar adsorption site (as final state) along four directions of the surface was calculated for each halogen. First, the structures of the initial and final states were optimized, and then the intermediate structures (16 structures) were calculated using DFT-D3, so that, at each iteration, the NEB method nudges the reaction path (atomic coordinates) towards the minimum energy geometry until convergence is reached. The 216-atom supercell used for calculating the diffusion barrier includes a nine-layer thick 4 × 6 Cu(110) slab and a 20 Å thick vacuum region. The bottom five layers in the Cu slab were fixed throughout the NEB calculations, while all of the other atomic coordinates were relaxed until all forces were smaller than 0.05 eV $Å^{-1}$.

Results and discussion

(1) Fast-XPS and reaction overview

On-surface Ullmann coupling is a two-step reaction,[28,52,53] with the formation of an OM intermediate and metal halide by-product in the first step, followed by the formation of a C–C bond in the second, rate-limiting step. As such, the nature of the halide is not generally considered to affect the overall rate of reaction. However, we show below that the C–C coupling step is in fact halogen-dependent (Fig. 1 and 4). The role of the halogen is manifested in the OM chain termination

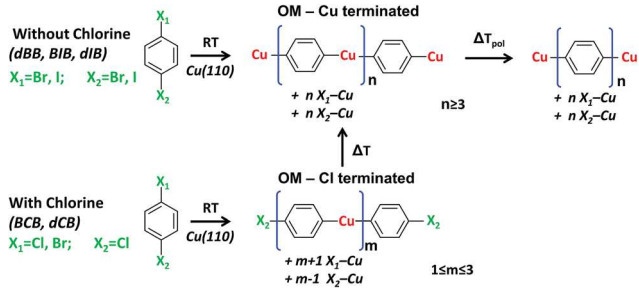

Fig. 1 Reaction schemes for dihalobenzene polymerizations. dBB, BIB and dIB on Cu(110) follow a two-step reaction forming an OM intermediate at RT, and polymers at higher temperatures. Chlorine-containing precursors (BCB and dCB) first form short OM chains due to incomplete dehalogenation of Cl at RT. Increasing the temperature results in a complete dehalogenation, forming longer OM chains. The polymerization step of the reaction is the same for all the five precursors. *m* and *n* represent the OM chain size.

at RT, in which the partial dehalogenation of the chlorine-containing molecules results in short chlorine-terminated OM chains, which change to Cu-terminated chains after dechlorination is completed at 150 °C. By contrast, the bromine- and iodine-containing molecules produce longer Cu-terminated chains at RT (Fig. 1).

The chemical states of the different carbon species involved in the dehalogenation and polymerization processes can be identified by measurement of the C 1s photoemission spectra, as reported in Fig. 2. At RT, the C 1s spectra are dominated by a main peak corresponding to the four closely equivalent sp^2 carbon atoms (C–C) at a binding energy (BE) of approximately 284.0 eV. The dehalogenated carbon atoms bound to Cu surface adatoms (C–Cu), give their contribution at a lower BE (283.3 eV). In the case of chlorinated molecules, the whole C 1s spectrum is shifted (0.3–0.4 eV) towards a higher BE, in which an additional minority component is detected at 285.5 eV, which we attribute to the intact C–Cl component. Similar to the bromine-containing molecules, the C 1s spectrum of the BCB precursor contains a shoulder at a lower BE, which is characteristic of Br dehalogenation. In the case of the doubly chlorinated molecule (dCB), the similar C–Cu component at the lower BE is clearly detected, thus suggesting a partial Cl dehalogenation. This weak component is more resolved at higher temperature (150 °C) when Cl dehalogenation is completed.

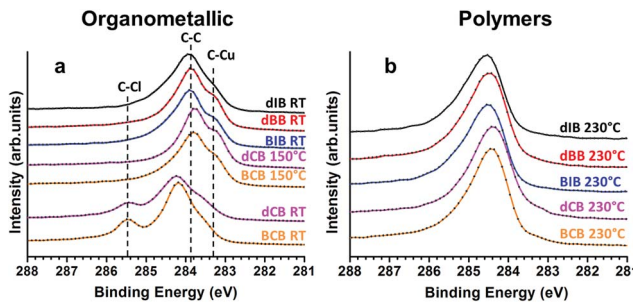

Fig. 2 C 1s spectra for saturated coverage of each precursor on Cu(110) for the organometallic (a) and polymer (b) phases.

This observation is consistent with the Cl 2p and Br 3d spectra of BCB reported in Fig. 3. The doublet Br 3d peak at 68.4 eV BE is in agreement with the dehalogenated C–Br at RT and 150 °C, whereas the (mostly) undissociated C–Cl is confirmed by only one doublet at ~200.0 eV (Cl $2p_{3/2}$) at RT. The dCB, on the other hand, has undergone nearly 50% of C–Cl dehalogenation at RT. as indicated by the additional doublet at a much lower BE of 198.0 eV, associated with Cl atoms directly bound to the Cu surface.

The evolution from the OM to polymeric phase for the five studied precursors was examined by acquiring fast-XPS spectra of the C 1s core level as a function of temperature. The fast-XPS maps presented in Fig. 4 show the differences for every precursor, indicating a halogen-dependent effect on the activation energy (starting temperature) and the kinetics (interval) of the corresponding reaction. All of

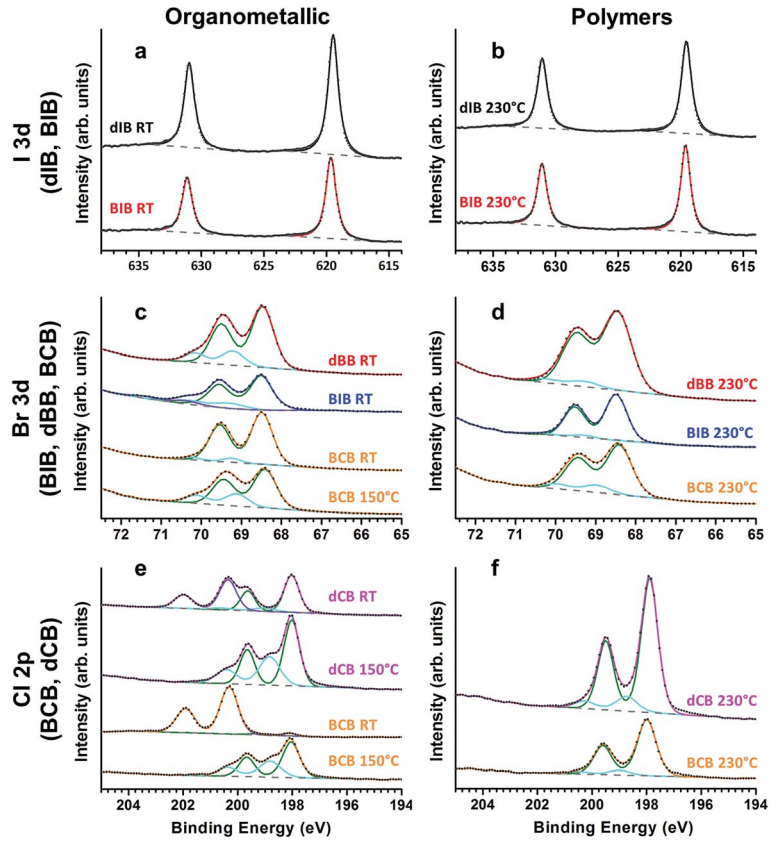

Fig. 3 XPS spectra (I 3d, Br 3d, Cl 2p) of organometallic (OM) (left panels, a, c, e) and polymer (right panels, b, d, f) chains for the saturated coverage of five precursors on Cu(110) at different temperatures. The component in green is attributed to the dissociated halogens, also observed for the spectra of the polymer chains. The component in light blue, observed for the long OM chains (dBB and BIB at RT, and BCB and dCB at 150 °C), is significantly reduced after polymerization. This component likely originates from the different adsorption sites of the halogens when long chains are present. For the Br 3d peak corresponding to BIB at RT, a weak component (in purple) is observed at 70.7 eV, attributed to a small fraction of intact C–Br bonds.

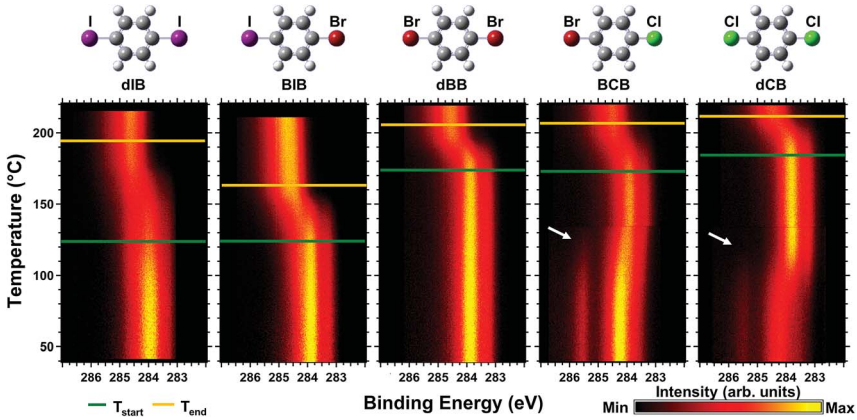

Fig. 4 Fast-XPS measurements of C 1s during annealing (0.2 °C s^{-1} heating rate) of a saturated monolayer of each precursor on Cu(110) dosed at RT. The temperatures at which 10% and 90% of the polymerization reaction is completed are marked with T_{start} (green) and T_{end} (orange) lines, respectively. White arrows indicate the change in the C 1s spectra due to C–Cl dissociation.

the fast-XPS maps exhibit a shift in the C 1s spectra towards a higher BE above 140 °C. This is a signature of polymerization, and is correlated with the progressive vanishing of the C–Cu component (at 283.3 eV) and growth of the C–C component at a higher BE,[28,37] shown in Fig. 2. The correlation of polymerization and the halogen type is seen in the starting temperature (T_{start}) of the conversion of OM to polymer, at 125 ± 2 °C for the dIB and BIB, at 175 ± 2 °C for dBB and BCB, and at 185 ± 2 °C for dCB, showing that T_{start} increases from the iodine- to the bromine- to the chlorine-containing molecules (green lines, Fig. 4). While for every molecule the reaction is completed within an approximately 40 °C range, the reaction for dIB proceeds across an 80 °C range (Table S1†). The final BE position of the main C 1s peak is found at 284.5 eV with small variations of ±0.1 eV between the various precursors, which remains within the experimental resolution.

The maps for chlorine-containing molecules present an earlier transition (than the OM-to-polymer conversion temperature range) at about 120 °C, witnessed by the C 1s shift towards lower BE, as highlighted by the white arrows in Fig. 4, which we can ascribe to the complete C–Cl dissociation. Full C–Br and C–I bond dehalogenation takes place below RT and, therefore, does not appear in the fast-XPS maps of the non-chlorinated precursors. The fast-XPS maps not only identify the critical temperature of the on-surface chemical reactions, but also highlight that the C–C coupling step of the reaction is halogen-dependent. For the iodine- and bromine-containing molecules, the scheme is similar to previous reports,[28,29,37,52] where a fully dehalogenated phase of OM chains forms at RT, and remains stable up to the polymerization temperature. For chlorine-containing molecules, the RT phase, which is stable up to 120 °C, is rather associated with the incomplete dehalogenation of dCB and BCB precursors. As a result, most of the phenyl groups would be Cl-terminated and form short OM chains on the surface (2 to 4 phenyls long). The XPS spectra for Cl 2p presented in Fig. 3e shows

that approximately 50% of the Cl–C bonds are dissociated for dCB, but only a small fraction for BCB.

C–Cl bond dissociation is completed at temperatures above 120 °C (Fig. 4), and longer chains are formed (>20 phenylenes long, as shown in Fig. 5). For dBB, BIB and dIB, the C–Br and C–I bonds are dissociated upon adsorption at RT on Cu(110), as can be seen from the Br 3d (Fig. 3c) and I 3d (Fig. 3a) spectra, in which their $3d_{5/2}$ components at 68.3 eV and 619.5 eV, respectively, are attributed to Cu–Br[28,29] and Cu–I bonds.[18] A single chemical state was observed for I 3d at every temperature during the reaction. For Br 3d and Cl 2p, the dominant states are found at 68.3 eV ($3d_{5/2}$) and 198.0 eV ($2p_{5/2}$), respectively, and additional components at higher BEs were observed at 69.1 eV (Br $3d_{5/2}$) and 198.8 eV (Cl $2p_{5/2}$) (Fig. 3c and e). In the case of dBB and BIB, these components were present at RT, while for the chlorine-containing molecules, they became apparent only after annealing to 150 °C, when dehalogenation is complete (Fig. 3e). The other chemical states (0.7 eV higher BE shift) in the Br 3d and Cl 2p spectra can be tentatively attributed to different adsorption sites of the halogen within the OM structure. The BIB spectra at RT exhibit a weak peak at 70.7 eV (Br $3d_{5/2}$), attributable to a minor fraction of Br–C bonds still being intact at RT.

Cleavage of the C–Br and C–I bonds occurs at lower temperatures, below the temperature range investigated in this study. For example, it is known that the dehalogenation of iodobenzene on Cu(110) takes place at approximately −100 °C.[23] Although the dissociation temperature of Br for bromobenzene or dBB

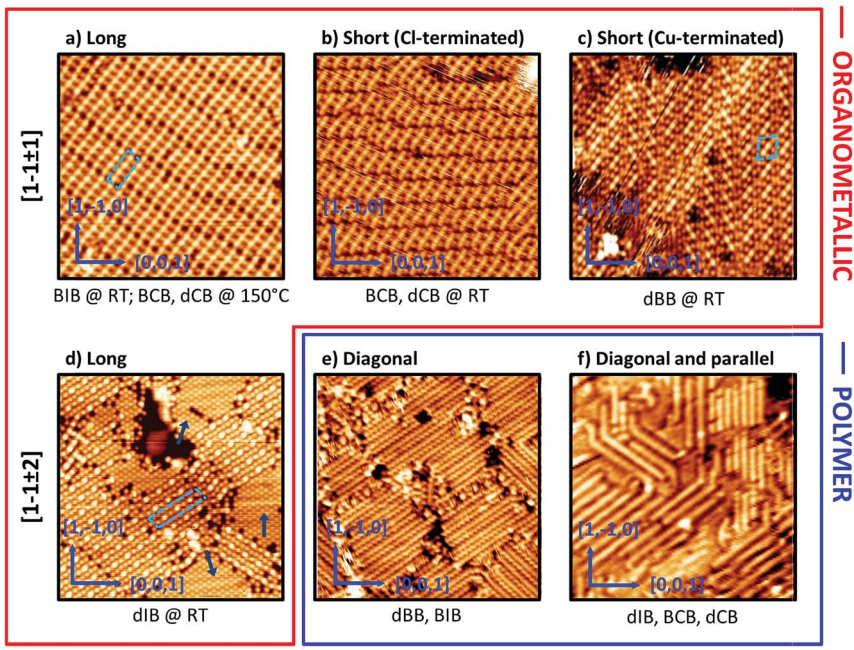

Fig. 5 STM images (20 × 20 nm^2) obtained for the five precursors on Cu(110). The OM phases (a–d) are shown in the red box; the blue arrows in (d) indicate the $c(2 \times 2)$ iodine superstructure; light blue dashed lines represent the molecular unit cells. BCB and dCB show two different OM phases at RT (b) and after annealing at 150 °C (a). The polymer phases (e and f), formed when annealing above 200 °C are presented in the blue box.

on Cu(110) is not available in the literature, the aryl halides (Ar–X) have shown a reactivity trend of Ar–I > Ar–Br > Ar–Cl. The dissociation of Br is therefore expected to happen at a higher temperature than iodine.[54,55] This trend agrees with DFT calculated dissociation energies of iodobenzene and bromobenzene,[20] and with the experimental values of the dissociation enthalpy of a Ph–halogen bond: 67 ± 2 kcal mol^{-1} for Ph–I, 84 ± 1 kcal mol^{-1} for Ph–Br and 97 ± 1 kcal mol^{-1} for Ph–Cl.[56]

A comparison of fast-XPS maps and XPS spectra between dIB and dBB is presented in Fig. S1.† dBB is taken as the representative of the other bromine- and chlorine-containing molecules (BIB, BCB and dCB) because their fast-XPS maps show similar behavior for the polymerization process, both in the temperature range of the polymerization reaction (Table S1,† temperature range) and in the OM chains, all along the same directions (Fig. 5). Fig. S1a and c† show the fast-XPS maps, where the C 1s line profiles at various temperatures through the ramp are shown every 20 °C in panels (b, d) (identical profiles have been omitted). While for dIB the shift is continuous and gradual toward higher BE values, it is sharp and sudden for dBB. STM images (Section 2) also show a clear difference between dBB and dIB structures on the surface, likely due to the fact that for dIB the OM chains are oriented along the same direction as the polymer, whereas for all other molecules this is not the case, as discussed in Section 2. Therefore, dIB coupling can happen for two monomers in an OM chain without affecting the other adjacent ones, *i.e.* the reaction can take place gradually, while for the other precursors a rotation is required for the phenyl–phenyl coupling, affecting the neighboring chains, which, we speculate, may require an additional barrier to be overcome for the monomers to couple.

(2) Structural characterization by STM

Deposition of each precursor on Cu(110) at RT results in distinctive self-assembled OM structures, oriented along different lattice directions, which produce poly(*para*-phenylene) (PPP) polymers upon annealing. The OM (red frame, Fig. 5a–d) and polymer (blue frame, Fig. 5e and f) structures obtained for the five precursors at different temperatures are shown in Fig. 5. The assignment of these phases is based on the distances between the protrusions in the STM data for the OM and polymer chains (6.3 Å and 4.4 Å, respectively),[28] together with the C 1s analysis described above.

Organometallic chains. All of the OM phases (Fig. 5a–d), appearing in two domains related by mirror symmetry with respect to the [1−10] direction, are made of chains of phenylene groups linked through copper atoms, and stacked into a 2D structure. The OM chains are oriented along either the [1−1±1] directions (Fig. 5a–c, dCB, BCB, dBB, BIB) or the [1−1±2] directions (Fig. 5d, dIB), and are interdigitated by rows of protrusions, identified as halogens.[28,57] For iodine-containing molecules, a portion of the surface is covered by the $c(2 \times 2)$ iodine superstructure (Fig. 5d). The directions of the molecular domains, together with the iodine superstructure, are shown in Fig. S2.† Higher resolution STM images of every phase for each precursor are presented in Fig. 6, superimposed with the proposed molecular structure. OM chains along the [1−1±2] directions are observed only for dIB, and are composed of ordered domains of long chains (limited only by the size of the terraces, defects and other domains), with

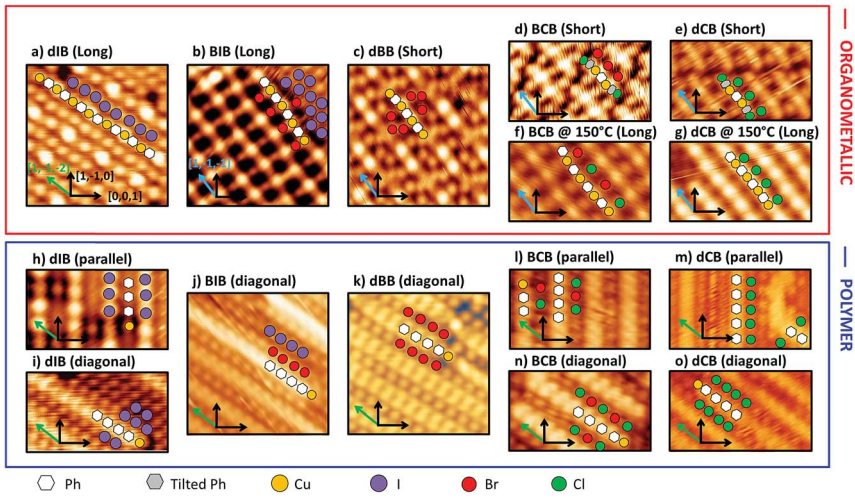

Fig. 6 STM images (square 5 × 5 nm^2, rectangular 2.5 × 5.0 nm^2) of the OM (a–e at RT and f and g at 150 °C) and polymeric phases (h–o at 230 °C) observed for each precursor, superimposed with molecular structures and copper lattice directions. OM chains for dIB (a) are orientated along the [1−1−2] direction, the same direction as the diagonal polymeric chains, while all the other OM chains are along the [1−1−1] direction.

a periodic strain-relieving kink every seven phenyls (Fig. S3†), and a surface reconstruction corresponding to the epitaxy matrices (1, −4|11, 10) and (1, 4|−11, 10). For the structures that produce [1−1±1]-oriented OMs, we observe two different types of chains: long (for BIB) and short (for dBB, BCB and dCB) at RT. The short chain structures are made of a smaller number of phenyls, between two to four for BCB and dCB (Fig. 5b) and exclusively three for dBB ('chevron' phase, Fig. 5c).[57] For dBB, the short chains are always Cu-terminated (Fig. 6c), while for BCB and dCB, they are Cl-terminated (Fig. 6d and e), as inferred from the XPS spectra in Fig. 3 showing complete debromination for dBB, as opposed to dechlorination for BCB and dCB. The presence of Cl at the chain-end forces the molecular aggregate to bend the terminal phenyls upwards, resulting in an apparent projected length in the STM profiles obtained along the [1−1−1] direction of the Cu–Ph–Cl group equal to 4.9 Å, which is shorter than the 6.4 Å known length of a Cu–Ph–Cu, as shown in Fig. S4a and b.† The reduced dichroism in the NEXAFS measurements support the hypothesis of partial lifting of some benzene rings (see Section 3). The RT structure for dBB is characterized by a longer-range order and described by epitaxy matrices (1, −4|6, 0) and (1, −1|4, 1).[37] An epitaxy matrix cannot be written for BCB and dCB at RT, due to a lack of long-range order.

The short OM phase of the chlorine-containing molecules presents a high mobility even at RT, as observed by consecutive STM images (one every minute), presented in ESI Video S1,† in which the orientation and domain size changes.

The dBB chevron phase is stable up to the polymerization temperature (175 °C), while the chain length of BCB and dCB increases when the dehalogenation process is completed at 150 °C, and long OM chains made of a higher number of phenyls (>20) are observed on the surface (Fig. S4d†). As for BIB at RT,

these chains comprise two domains along the [1−1±1] directions and have a periodic strain-relieving kink every four phenyls (Fig. S3†) and are described by the epitaxy matrices (2, −2|4, 9) and (2, 2|−4, 9).

The difference between the OM chain direction for dIB and that of the other molecules (BIB, dBB, BCB and dCB) can be inferred from the halogens' preferred adsorption site on Cu(110); iodine atoms occupy hollow sites,[18] while Br and Cl atoms are located at short-bridge sites (Fig. S3†).[28,29,58] STM line profiles of the halogen atoms between the OM chains show that for dIB, iodine atoms adsorb along the [1−1±2] directions, with a 4.4 Å periodicity and are located in hollow positions; while for the other molecules, Br and Cl atoms follow the [1−1±1] directions, with a 6.3 Å periodicity and are located at short-bridge positions. We can therefore suppose that in the BIB case, bromine atoms decorate the OM chains, while iodine atoms are segregated into the $c(2 \times 2)$ domains. At the boundaries between the $c(2 \times 2)$ domains and the OM chains, both Br and I atoms are located along the chains, with two atoms in hollow positions and one atom at a short-bridge position (Fig. S5†).

Polymer chains. The polymer phase (Fig. 5e and f), is made of linear chains of π-conjugated phenyls decorated with halogen atoms. dBB and BIB exclusively produce polymers along the direction [1−1±2] (the 'diagonal' direction of the Cu(110) surface unit cell), while BCB, dCB and dIB show polymers along both the diagonal [1−1±2] and 'parallel' (to the Cu(110) close-packed row, [1−10]) directions. The phenyl–phenyl distance is 4.4 Å for all of the polymers, a distance which is commensurate with the diagonal direction and incommensurate for the parallel direction.[57] Commensurability with the surface permits diagonal polymers to grow with no strain penalty, and results in the formation of large islands of polymers with a mean length greater than 20 phenyl units. However, the electronic properties are strictly related to the polymer length,[14,57] and whether a particular halogen or an intermediate phase favors longer chains is therefore important for selecting the right building block.

(3) NEXAFS and molecular orientation

C K-edge NEXAFS spectra obtained at RT as a function of the photon's polarization direction for all precursors (Fig. 7) present two π* transitions, π_1^* and π_2^* at ∼284.5 and ∼288.5 eV, respectively, in agreement with the cases of dBB on Cu(110)[28] and halobenzenes on Cu(111).[59] These spectra show that the phenyl rings are mostly flat on the surface, supporting the orientational hypotheses derived from the STM images. The C K-edge NEXAFS spectra at RT for chlorine-containing molecules show higher tilt of the phenyl ring, according to the change in the intensity of the π* states as a function of the polarization vector direction of incoming photons with respect to the surface normal, particularly for π_2^* resonance (black line in Fig. 7), where a peak is visible for $\theta = 0^\circ$.[60] This feature is not present for the non-chlorinated molecules at RT (Fig. 7a), and is consistent with a fraction of the molecules being tilted away from the surface. We additionally note the presence of a shoulder on the high-energy side of the π_1^* resonance at $\theta = 90^\circ$ (Fig. 7b), a feature not observed for the other precursors. After annealing to 150 °C, the intensity of the π_2^* resonance at $\theta = 0^\circ$ for dCB and BCB is strongly suppressed, and the spectra in all polarizations become qualitatively indistinguishable from the RT spectra observed for the other molecules. This is

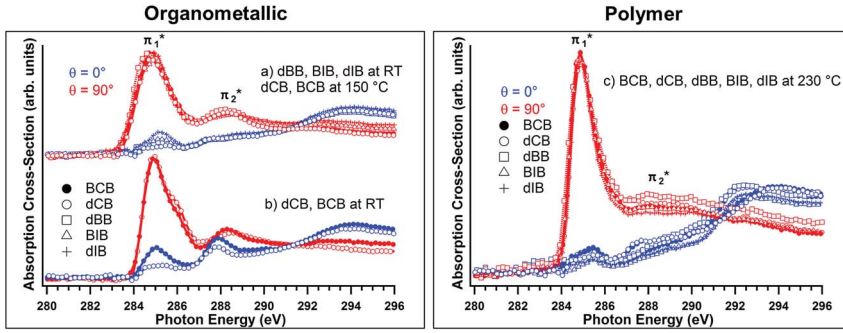

Fig. 7 Polarization-dependent C K-edge NEXAFS spectra for the five studied precursors; (a) dBB, BIB and dIB at RT and BCB and dCB at 150 °C; (b) dCB and BCB at RT and (c) all precursors at 230 °C. For each sample we report $\theta = 90°$ (red, TM geometry, close to p-polarization) and $\theta = 0°$ (blue, TE geometry, s-polarization) with the incident radiation falling in the plane containing the normal sample and the [1−10] lattice direction. Single spectra for each precursor are presented in Fig. S6 and S7.†

consistent with the STM data, where OM structures along the same directions are observed for all molecules but dIB, and the C 1s XPS data, where the spectra are identical for dCB and BCB at 150 °C and dIB, BIB and dBB at RT (Fig. 2). Annealing all of the precursors to 230 °C completely suppresses the π_2^* resonance intensity, indicating the planarity of the aromatic rings, expected for the PPP polymers (Fig. 7 and S7†).[28,29,61]

(4) Role of the halogen in the reaction

The halogen might affect the reaction mechanism and the barrier energies in a variety of ways. Here, we present two hypotheses based on (i) the effect of differing diffusion barriers for the halogens, and (ii) the possible presence of the halogen atoms on-top of the copper atoms in the OM structure. The hypotheses are not mutually exclusive and the observed behaviour could contain contributions from both effects.

To explore the first hypothesis, NEB calculations for the diffusion of the halogens along different directions of the Cu(110) surface were performed ([001], [1−10], [1−11] and [1−12]). These simulations consider the diffusion of the halogen alone and use a hollow position as the starting position for I atoms and a short-bridge position as the starting position for Br and Cl atoms, known to be the respective preferred adsorption site for the halogens.[58,62–64] The overall trend of the diffusion energy as I < Br < Cl (Fig. 8) is consistent with the starting temperature of the OM-to-polymer conversion reaction found in the fast-XPS maps (Fig. 4), where the polymerization of dCB starts at the highest temperature, and at the lower temperature for iodine-containing molecules. Unlike chlorine and bromine, the diffusion barrier for iodine along the [1−12] direction is higher than the other two directions. This could be explained by the diffusion of iodine along the [1−12] direction, which needs to pass from a stable hollow adsorption site to an on-top location on the Cu surface. Therefore, having the lower diffusion energy barriers along the other two directions, the iodine atoms can make a two-step movement, along [1−10] and [001], instead of diffusing

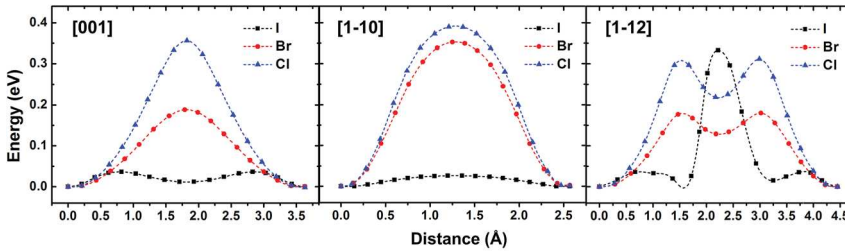

	E_d[001] (eV)	E_d[1-10] (eV)	E_d[1-12] (eV)
Cl	0.36	0.39	0.31
Br	0.19	0.35	0.18
I	0.04	0.03	0.33

Fig. 8 (Top panels) NEB plots of the minimum energy path for the diffusion of iodine, bromine and chlorine along one unit cell in the [1−10], [001] and [1−12] directions of Cu(110). For Br and Cl, the starting equilibrium position is short-bridge, while for I it is hollow. (Bottom panel) Diffusion energies (E_d) for I, Br and Cl along the studied directions.

directly through the [1−12]. The molecular structures for local maxima and minima of the paths are presented in the ESI (Fig. S8–11†), together with the calculations for the diffusion along the [1−11] direction. We can further speculate that a lower diffusion barrier for the halogens also facilitates monomer diffusion, thereby reducing the transition temperature. Conversely, a higher diffusion barrier for the halogens requires an overall higher temperature for the polymerization to occur, as observed experimentally.

The second hypothesis is connected with the halogen being integrated into portions of the OM chains, as proposed by Di Giovannantonio *et al.*[28,29] In this work Br atoms were proposed to occupy two different positions of the unit cell of OM chains for dBB on Cu(110), four per unit cell on the short-bridge lattice site between adjacent OM chains, and four adsorbed on top of the Cu atoms forming the OM (*i.e.* between the phenyls). This hypothesis is based on simulated STM images, which show a better qualitative match with the experimental STM images when top Br atoms are included. To complete the polymerization reaction, the copper atoms in the OM structure need to be expelled from the chains to permit covalent binding between adjacent phenyls. If a halogen atom is present on top of these Cu atoms, the energies involved in the polymerization reaction must depend on the type of halogen, and will result in a different temperature for the reaction depending on the type of precursor.

Conclusions and perspectives

The role of the halogen in the Ullmann coupling polymerization of five 1,4-dihalobenzene precursors containing Cl, Br, and I on Cu(110) was studied using combined fast-XPS, NEXAFS and STM analysis. On one hand, the nature of the halogen atom, hence the strength of its bond to carbon atoms, affects the temperature of the dehalogenation step. On the other hand, the type of halogen drives the geometry of the OM structures obtained at RT as well as the orientation

of the polymers. In fact, (i) the length of the OM chains depends on the carbon–halogen bond dissociation energy, and (ii) the OM structures for precursors containing Br and Cl (dBB, dCB, BCB, BIB) are aligned along the [1−1±1] directions, as opposed to alignment along the [1−1±2] directions for precursors containing only iodine (dIB). The OM structures follow different reaction kinetics, exhibiting a gradual transition for dIB while the others undergo a sudden transition into PPP polymers. A key finding of this study is that the temperature range of the polymerization is affected by the type of halogen, and is qualitatively correlated to the halogen's diffusion energy. Our results show that the halogen is not merely a reaction by-product, but rather an important parameter governing the on-surface Ullmann polymerization reaction.

Statement of author contributions

J. L. D, D. F. P., F. R. and G. C. conceived the project. G. G., M. D. G. and S. T. performed the STM experiments, and with the supervision of J. L. D. and M. E. Y. F. R. participated in the analysis of the STM images. G. G., M. D. G., J. L. D. and G. C. performed NEXAFS and fast-XPS experiments at the Elettra synchrotron. A. V. and L. F. assisted with synchrotron measurements at the Aloisa beamline. M. E. performed the theoretical calculations. G. G. wrote the manuscript, together with M. E. and G. C. All of the authors commented critically on the manuscript.

Conflict of interest

The authors declare no competing financial interest.

Acknowledgements

This work is partially supported by the Italy-France International Program of Scientific Cooperation (PICS CNR-CNRS). G. C. and F. R. acknowledge support from CNR through Short-term Mobility (STM) Fellowships. The authors acknowledge beamtime access and support from the Elettra light source in Italy. F. R. and D. F. P. are supported by NSERC through individual Discovery Grants as well as the Fonds québécois de la recherche sur la nature et les technologies (FQNRT) through a Team Grant, and the Ministère du Développement Économique, de l'Innovation et de l'Exportation (MDEIE) through a Collaboration Grant. F. R. is also grateful to the Canada Research Chair program for funding and partial salary support. G. G. is grateful to G. Vasseur and M. El Garah for their participation in collecting the STM images. Computations were performed on the tcs supercomputer at the SciNet HPC Consortium, funded by the Canada Foundation for Innovation under Compute Canada, the Government of Ontario, Ontario Research Fund – Research Excellence, and the University of Toronto. Some of the simulated structures in the SI are presented using VESTA software.

Notes and references

1 K. S. Novoselov, A. K. Geim, S. V. Morozov, D. Jiang, Y. Zhang, S. V. Dubonos, I. V. Grigorieva and A. A. Firsov, *Science*, 2004, **306**, 666–669.
2 C. Lee, X. Wei, J. W. Kysar and J. Hone, *Science*, 2008, **321**, 385–388.

3 A. H. Castro Neto, F. Guinea, N. M. R. Peres, K. S. Novoselov and A. K. Geim, *Rev. Mod. Phys.*, 2009, **81**, 109–162.
4 F. Bonaccorso, Z. Sun, T. Hasan and A. C. Ferrari, *Nat. Photonics*, 2010, **4**, 611–622.
5 M. Ebrahimi and F. Rosei, *Nature*, 2017, **542**, 423–424.
6 W. Liu, X. Luo, Y. Bao, Y. P. Liu, G.-H. Ning, I. Abdelwahab, L. Li, C. T. Nai, Z. G. Hu, D. Zhao, B. Liu, S. Y. Quek and K. P. Loh, *Nat. Chem.*, 2017, **9**, 563–570.
7 F. J. Uribe-Romo and W. R. Dichtel, *Nat. Chem.*, 2012, **4**, 244–245.
8 S. E. Thompson and S. Parthasarathy, *Mater. Today*, 2006, **9**, 20–25.
9 M. El Garah, J. M. MacLeod and F. Rosei, *Surf. Sci.*, 2013, **613**, 6–14.
10 D. F. Perepichka and F. Rosei, *Science*, 2009, **323**, 216–217.
11 J. Sakamoto, J. van Heijst, O. Lukin and A. D. Schlüter, *Angew. Chem., Int. Ed.*, 2009, **48**, 1030–1069.
12 N. R. Champness, *Nat. Chem.*, 2012, **4**, 149–150.
13 J. W. Colson and W. R. Dichtel, *Nat. Chem.*, 2013, **5**, 453–465.
14 R. Gutzler and D. F. Perepichka, *J. Am. Chem. Soc.*, 2013, **135**, 16585–16594.
15 J. Liu, B.-W. Li, Y.-Z. Tan, A. Giannakopoulos, C. Sanchez-Sanchez, D. Beljonne, P. Ruffieux, R. Fasel, X. Feng and K. Müllen, *J. Am. Chem. Soc.*, 2015, **137**, 6097–6103.
16 R. Gutzler, *Phys. Chem. Chem. Phys.*, 2016, **18**, 29092–29100.
17 M. Di Giovannantonio, T. Kosmala, B. Bonanni, G. Serrano, N. Zema, S. Turchini, D. Catone, K. Wandelt, D. Pasini, G. Contini and C. Goletti, *J. Phys. Chem. C*, 2015, **119**, 19228–19235.
18 J. Lipton-Duffin, O. Ivasenko, D. Perepichka and F. Rosei, *Small*, 2009, **5**, 592–597.
19 L. Grill, M. Dyer, L. Lafferentz, M. Persson, M. V. Peters and S. Hecht, *Nat. Nanotechnol.*, 2007, **2**, 687–691.
20 J. Björk, F. Hanke and S. Stafström, *J. Am. Chem. Soc.*, 2013, **135**, 5768–5775.
21 L. Lafferentz, V. Eberhardt, C. Dri, C. Africh, G. Comelli, F. Esch, S. Hecht and L. Grill, *Nat. Chem.*, 2012, **4**, 215–220.
22 A. Basagni, L. Colazzo, F. Sedona, M. DiMarino, T. Carofiglio, E. Lubian, D. Forrer, A. Vittadini, M. Casarin, A. Verdini, A. Cossaro, L. Floreano and M. Sambi, *Chem.–Eur. J.*, 2014, **20**, 14296–14304.
23 M. Xi and B. E. Bent, *J. Am. Chem. Soc.*, 1993, **115**, 7426–7433.
24 S.-W. Hla, L. Bartels, G. Meyer and K.-H. Rieder, *Phys. Rev. Lett.*, 2000, **85**, 2777–2780.
25 S. Schlögl, W. M. Heckl and M. Lackinger, *Surf. Sci.*, 2012, **606**, 999–1004.
26 R. Gutzler, H. Walch, G. Eder, S. Kloft, W. M. Heckl and M. Lackinger, *Chem. Commun.*, 2009, 4456–4458, DOI: 10.1039/b906836h.
27 M. Bieri, M. T. Nguyen, O. Groning, J. M. Cai, M. Treier, K. Ait-Mansour, P. Ruffieux, C. A. Pignedoli, D. Passerone, M. Kastler, K. Mullen and R. Fasel, *J. Am. Chem.Soc.*, 2010, **132**, 16669–16676.
28 M. Di Giovannantonio, M. El Garah, J. Lipton-Duffin, V. Meunier, L. Cardenas, Y. Fagot Revurat, A. Cossaro, A. Verdini, D. F. Perepichka, F. Rosei and G. Contini, *ACS Nano*, 2013, **7**, 8190–8198.
29 M. Di Giovannantonio, M. El Garah, J. Lipton-Duffin, V. Meunier, L. Cardenas, Y. Fagot-Revurat, A. Cossaro, A. Verdini, D. F. Perepichka, F. Rosei and G. Contini, *ACS Nano*, 2014, **8**, 1969–1971.

30 J. Eichhorn, T. Strunskus, A. Rastgoo-Lahrood, D. Samanta, M. Schmittel and M. Lackinger, *Chem. Commun.*, 2014, **50**, 7680–7682.
31 L. Cardenas, R. Gutzler, J. Lipton-Duffin, C. Fu, J. L. Brusso, L. E. Dinca, M. Vondráček, Y. Fagot-Revurat, D. Malterre and F. Rosei, *Chem. Sci.*, 2013, **4**, 3263–3268.
32 L. Leung, T. Lim, Z. Ning and J. C. Polanyi, *J. Am. Chem. Soc.*, 2012, **134**, 9320–9326.
33 A. Eisenstein, L. Leung, T. Lim, Z. Ning and J. C. Polanyi, *Faraday Discuss.*, 2012, **157**, 337–353.
34 M. Chen, J. Xiao, H.-P. Steinrück, S. Wang, W. Wang, N. Lin, W. Hieringer and J. M. Gottfried, *J. Phys. Chem. C*, 2014, **118**, 6820–6830.
35 M. Xi and B. E. Bent, *Surf. Sci.*, 1992, **278**, 19–32.
36 J. M. Meyers and A. J. Gellman, *Surf. Sci.*, 1995, **337**, 40–50.
37 M. Di Giovannantonio, M. Tomellini, J. Lipton-Duffin, G. Galeotti, M. Ebrahimi, A. Cossaro, A. Verdini, N. Kharche, V. Meunier, G. Vasseur, Y. Fagot-Revurat, D. F. Perepichka, F. Rosei and G. Contini, *J. Am. Chem. Soc.*, 2016, **138**, 16696–16702.
38 J. Björk, *J. Phys.: Condens. Matter*, 2016, **28**, 083002.
39 I. Horcas, R. Fernandez, J. Gomez-Rodriguez, J. Colchero, J. Gómez-Herrero and A. Baro, *Rev. Sci. Instrum.*, 2007, **78**, 013705.
40 N. Fairley, *CasaXPS Manual 2.3.15: Introduction to XPS and AES*, Casa Software, 2009.
41 G. Contini and S. Turchini, *Comput. Phys. Commun.*, 1996, **94**, 49–52.
42 L. Floreano, A. Cossaro, R. Gotter, A. Verdini, G. Bavdek, F. Evangelista, A. Ruocco, A. Morgante and D. Cvetko, *J. Phys. Chem. C*, 2008, **112**, 10794–10802.
43 G. Kresse and J. Hafner, *Phys. Rev. B: Condens. Matter Mater. Phys.*, 1993, **47**, 558–561.
44 G. Kresse and J. Furthmüller, *Phys. Rev. B: Condens. Matter Mater. Phys.*, 1996, **54**, 11169–11186.
45 L. Chris, G. Daniel, G. Leslie, P. Richard, B. Neil, C. Michael, H. Teresa, D. Jillian, Y. Ching-Hsing, C. Joseph, L. J. Dursi, C. Jason, N. Scott, P. Jaime, K. Neil and Z. Ramses Van, *J. Phys.: Conf. Ser.*, 2010, **256**, 012026.
46 J. P. Perdew, M. Ernzerhof and K. Burke, *J. Chem. Phys.*, 1996, **105**, 9982–9985.
47 P. E. Blöchl, *Phys. Rev. B: Condens. Matter Mater. Phys.*, 1994, **50**, 17953–17979.
48 G. Kresse and D. Joubert, *Phys. Rev. B: Condens. Matter Mater. Phys.*, 1999, **59**, 1758–1775.
49 S. Grimme, J. Antony, S. Ehrlich and H. Krieg, *J. Chem. Phys.*, 2010, **132**, 154104.
50 G. Henkelman, B. P. Uberuaga and H. Jónsson, *J. Chem. Phys.*, 2000, **113**, 9901–9904.
51 G. Henkelman and H. Jónsson, *J. Chem. Phys.*, 2000, **113**, 9978–9985.
52 W. Wang, X. Shi, S. Wang, M. A. Van Hove and N. Lin, *J. Am. Chem. Soc.*, 2011, **133**, 13264–13267.
53 K. J. Shi, D. W. Yuan, C. X. Wang, C. H. Shu, D. Y. Li, Z. L. Shi, X. Y. Wu and P. N. Liu, *Org. Lett.*, 2016, **18**, 1282–1285.
54 T. D. Sheppard, *Org. Biomol. Chem.*, 2009, **7**, 1043–1052.
55 J. L. Lin and B. E. Bent, *J. Phys. Chem.*, 1992, **96**, 8529–8538.
56 S. J. Blanksby and G. B. Ellison, *Acc. Chem. Res.*, 2003, **36**, 255–263.

57 G. Vasseur, Y. Fagot-Revurat, M. Sicot, B. Kierren, L. Moreau, D. Malterre, L. Cardenas, G. Galeotti, J. Lipton-Duffin, F. Rosei, M. Di Giovannantonio, G. Contini, P. Le Fèvre, F. Bertran, L. Liang, V. Meunier and D. F. Perepichka, *Nat. Commun.*, 2016, **7**, 10235.
58 B. V. Andryushechkin, K. N. Eltsov and V. M. Shevlyuga, *Surf. Sci.*, 2005, **584**, 278–286.
59 M. X. Yang, M. Xi, H. Yuan, B. E. Bent, P. Stevens and J. M. White, *Surf. Sci.*, 1995, **341**, 9–18.
60 J. Stöhr, *NEXAFS spectroscopy*, Springer-Verlag, Berlin, Heidelberg, 1992.
61 J. Novak, M. Oehzelt, S. Berkebile, M. Koini, T. Ules, G. Koller, T. Haber, R. Resel and M. G. Ramsey, *Phys. Chem. Chem. Phys.*, 2011, **13**, 14675–14684.
62 J. L. Stickney, C. B. Ehlers and B. W. Gregory, *Langmuir*, 1988, **4**, 1368–1373.
63 L.-J. Wan and K. Itaya, *J. Electroanal. Chem.*, 1999, **473**, 10–18.
64 B. V. Andryushechkin, in *Surf. Interface Sci.*, ed. K. Wandelt, Wiley-VCH Verlag GmbH & Co. KGaA, Weinheim, Germany, 2016, vol. 5, ch. 35, pp. 207–254.